JGR Atmospheres

RESEARCH ARTICLE
10.1029/2020JD033139

On the Isotopic Composition of Cold Pools in Radiative-Convective Equilibrium

Giuseppe Torri[1]

[1]Department of Atmospheric Sciences, University of Hawai'i at Mānoa, Honolulu, HI, USA

Key Points:

- Rain evaporation and equilibration effects deplete downdrafts in their initial stages and enrich them near the surface
- Latent heat fluxes play a greater role than mixing in enriching cold pools throughout their life cycle
- Stable water isotopologues could be used to diagnose the origin of water vapor in cold pool moist patches, but the signal may be small

Supporting Information:

Supporting Information may be found in the online version of this article.

Correspondence to:

G. Torri,
gtorri@hawaii.edu

Citation:

Torri, G. (2021). On the isotopic composition of cold pools in radiative-convective equilibrium. *Journal of Geophysical Research: Atmospheres*, *126*, e2020JD033139. https://doi.org/10.1029/2020JD033139

Received 21 MAY 2020
Accepted 19 MAR 2021

Abstract Although stable water isotopologues are important tools in the study of the climate system, some of the physical processes that affect them are still imperfectly constrained. In this work, I concentrate on cold pools, essential components of deep convective systems that are arguably one of the least understood features from the water isotopologue perspective. Using a combination of a Lagrangian and an Eulerian framework, I first focus on quantifying how different processes determine the initial water vapor isotopic composition of cold pools. By analyzing the precipitation-driven downdrafts that give rise to cold pools, I determine that mixing with environmental air has an enriching effect. On the other hand, microphysical processes tend to deplete the downdraft in the initial stages, mostly in the free troposphere, and to enrich it in the final stages, when the downdraft is in the subcloud layer. Then, I consider what processes might influence the isotopic composition of cold pools during their propagation, and I find that surface latent heat fluxes play a much greater role than cold pool entrainment. Finally, I show how water isotopologues could be used to diagnose the origin of water vapor in cold pool moist patches.

Plain Language Summary Water molecules exist in different species, called isotopologues, each containing different combinations of lighter and heavier varieties, or isotopes, of hydrogen and oxygen. Because these differences give molecules different chemical and physical properties, water isotopologues can reveal important information on the history of each air parcel and the physical processes that affected it. Here, I focus on cold pools, which are air currents near the surface that are generated by storms. Using computer simulations, I analyze how physical processes, such as the evaporation of rain or mixing between cold pools and air in the environment, affect the isotopes in cold pool water vapor.

1. Introduction

Cumulus clouds are a fundamental component of the Earth's climate. They strongly impact the radiation budget, hydrological processes, and transport of heat, momentum, and various chemical species. Uncertainties in our understanding of cumulus clouds and their interactions with the larger scales have important repercussions, for example, in future projections and estimates of climate sensitivity derived from model simulations (e.g., Zhao et al., 2016). Indeed, the representation of cumulus clouds in numerical models remains an outstanding challenge in climate science (Arakawa, 2004; Siebesma et al., 2020).

Stable water isotopologues have proved to be important tools to better understand and constrain processes regarding cumulus clouds and, more generally, atmospheric convection (e.g., Bailey, 2020; Bailey et al., 2015, 2017; Benetti et al., 2018; Conroy et al., 2016; Dee et al., 2018; Dütsch et al., 2018; Galewsky, 2018; Guilpart et al., 2017; Kurita et al., 2011; Noone, 2012; Noone et al., 2011; Nusbaumer et al., 2017; Risi et al., 2020, 2019; Torri et al., 2017). Differences in their masses provide isotopes of a given element with slightly different physical and chemical properties. In turn, this implies that certain processes can affect the relative abundance of isotopes in a given sample, something known as *isotope fractionation*. In the case of atmospheric convection, measuring and tracking the evolution of isotope abundances in an air parcel could thus reveal important insights on its history and on which processes affected it. Bailey et al. (2015), for example, used data on water vapor isotopes collected on Hawai'i Island to constrain convective precipitation efficiency, an important parameter with a strong influence on future climate projections and that is hard to constrain (Lutsko & Cronin, 2018). To cite another example, isotope ratios were also utilized to measure the

proportions of convective to stratiform precipitation, thus providing an additional constraint that could be used to improve climate models (Aggarwal et al., 2016; Chang et al., 2020).

Recently, considerable effort has been put in the study of water vapor isotopes in the lower troposphere and the boundary layer. Convective processes in lower parts of the troposphere can explain a substantial part of the variance in climate model estimates of equilibrium climate sensitivity (Bony et al., 2015; Sherwood et al., 2014). In this context, for example, water vapor isotopes were used to constrain mixing between the boundary layer and the lower troposphere (Bailey et al., 2013; Galewsky, 2015; Galewsky & Rabanus, 2016; Benetti et al., 2018; Feng et al., 2019; Risi et al., 2019), or to constrain the humidity of the subtropical troposphere (Galewsky et al., 2007; González et al., 2016; Guilpart et al., 2017; Hurley et al., 2012; Noone, 2012; Noone et al., 2011).

Most of the studies that focused on water vapor isotopes in the boundary layer have either considered quiescent-weather cases or used single-column models in which convection is parameterized. As a result, the influence of many convective processes on boundary layer isotopes is not well understood. An example which illustrates this knowledge gap is provided by dynamical features of deep convective systems known as cold pools, which are gravity currents generated by the injection of evaporatively-cooled downdraft air into the boundary layer. Among other things, cold pools are hypothesized to be crucial in explaining the diurnal cycle of convection, particularly the transition from shallow to deep convection (e.g., Böing et al., 2012; Khairoutdinov & Randall, 2006; Kuang & Bretherton, 2006; Rio et al., 2009; Schlemmer & Hohenegger, 2014; Tompkins, 2001), something that General Circulation Models (GCMs) often have difficulty representing correctly (Bechtold et al., 2004; Betts & Jakob, 2002; Yang & Slingo, 2001).

As they evolve in the boundary layer, cold pools develop positive water vapor anomalies at their edges, called moist patches (de Szoeke et al., 2017; Drager et al., 2020; Zuidema et al., 2017). Air that originates from these patches experiences a reduced convective inhibition and, therefore, has a thermodynamic advantage compared to other parcels in the boundary layer (Tompkins, 2001). Using numerical models, it was shown that this mechanism could explain how cold pools trigger new convective cells in environments with low wind shear and relatively weak cold pools (Tompkins, 2001; Torri et al., 2015). Despite their importance, moist patches and the related triggering mechanism are not included in the convective schemes used in GCMs and remain poorly constrained, both in observations (Chandra et al., 2018), and in model simulations (Langhans & Romps, 2015; Li et al., 2014; Schlemmer & Hohenegger, 2016; Seifert & Heus, 2013; Tompkins, 2001; Torri & Kuang, 2016b).

Cold pools can also impact water isotopologues in the atmosphere. For example, Risi et al. (2020) suggest that, by affecting the initial isotopic composition of convective updrafts, cold pools could play a significant role in explaining the amount effect, the empirical observation that, on sufficiently long time scales, the isotopic composition of rainfall is anticorrelated with the rainfall rate (Dansgaard, 1964; Kurita, 2013; Lee & Fung, 2008; Moore et al., 2014; Risi et al., 2008). Clarifying the behavior of water vapor isotopes in cold pools can therefore be beneficial to the understanding of water isotopologues in the boundary layer as well as in the free troposphere. Ultimately, this could provide more confidence in the use of water isotopologues to constrain important climate processes.

In this work, I will focus on cold pools and seek a process-based understanding of what controls their isotopic composition. In Section 2, I will introduce the isotope-enabled Cloud Resolving Model (CRM) and the Lagrangian Particle Dispersion Model (LPDM) used for this study. In Section 3, I will present results on how microphysical processes and mixing affect the isotopic composition of the downdrafts that generate cold pools, and how latent heat fluxes and mixing affect the composition of cold pools while they propagate. In addition, I will show how water vapor isotopes could be used as a means to diagnose the source of water vapor in moist patches. In Sections 4 and 5, I will discuss the implications and the limitations of this work.

2. Methods

2.1. The Model

The CRM used to conduct the simulations discussed in this work is the System for Atmospheric Modeling (SAM), version 6.8.2 (Khairoutdinov & Randall, 2003). The model solves the anelastic equations of

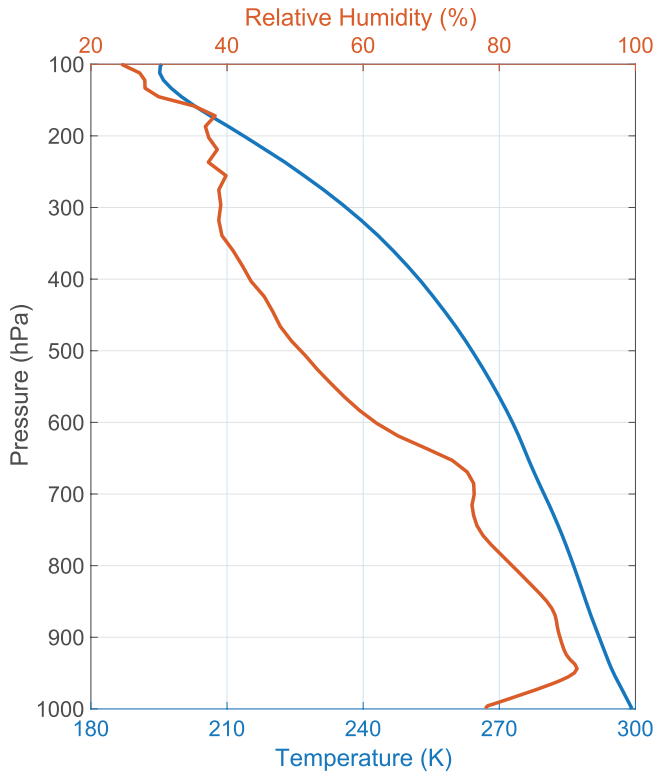

Figure 1. Horizontal and temporal averages of temperature (blue) and relative humidity (red) as a function of pressure.

motion, and uses liquid water static energy and nonprecipitating and precipitating total water as prognostic variables. The equations of motion are solved with doubly periodic boundary conditions in the horizontal directions and a rigid lid on top, with a sponge layer in the upper third of the domain to absorb gravity waves reflected from the top. A prognostic turbulent kinetic energy 1.5-order closure scheme is used to parameterize subgrid scale effects. Surface sensible and latent heat fluxes are computed using the Monin-Obukhov formula assuming an oceanic surface with sea surface temperature (SST) fixed at 301.15 K. Radiative processes are parameterized using the CAM3 scheme (Collins et al., 2006), whereas the microphysical processes are represented using the scheme described in Blossey et al. (2010). That microphysics scheme is based on a modified version of the single-moment Lin scheme (Chen & Sun, 2002; Lin et al., 1983), which predicts the mixing ratios of water vapor, cloud liquid water, cloud ice, rain, snow, and graupel, the latter of which is a hydrometeor that forms when supercooled liquid droplets freeze on falling snowflakes. The scheme used in this study also includes fractionation processes for water isotopologues. A more detailed description of this scheme, including all the modifications with respect to the Lin scheme, can be found in Blossey et al. (2010). For simplicity, I refer to this modified version of SAM as SAMiso.

The simulations are conducted over a domain measuring 96 × 96 km^2 horizontally and 30 km vertically. The horizontal grid spacing is 250 m, while vertically it varies continuously from a minimum of 31 m up to 500 m, the latter reached just above an altitude of 10 km, or 300 hPa. The model has 20 layers in the bottom 1 km of the domain. The time step is three seconds. The diurnal cycle is removed by fixing the zenith angle at 51.7° and decreasing the solar constant to 685 W m^{-2} (Tompkins & Craig, 1998). Mean winds are initialized at zero.

As mentioned in Section 1, some of the results presented in this work are obtained using the LPDM (e.g., Nie & Kuang, 2012; Torri et al., 2015), which I run online with SAMiso. The LPDM is initialized with 400 particles per column, their initial positions being randomly distributed in horizontal and pressure coordinates. At the beginning of the simulation, each particle is assigned three mixing ratios, one per water isotopologue (see Section 2.2). At each time step, these values are updated according to the tendencies that a particle experiences in the grid box it is contained in. These tendencies can either be due to microphysical processes, diffusion, or mixing with other particles in the same grid box (for a more detailed account, see the supporting information in Torri & Kuang, 2016b), and they are diagnosed from SAMiso. In formulae:

$$\frac{\delta q_v}{\delta t} = \left(\dot{q}_v\right)_{mic} + \left(\dot{q}_v\right)_{dif} + \left(\dot{q}_v\right)_{mix} \tag{1}$$

This is repeated for all isotopologues. By saving all three tendency terms for each particle at every time step, it is possible to reconstruct the entire history of water vapor isotopes for any particle, and assess the relative role of different physical processes in modulating their mixing ratios.

I first run SAMiso for 50 days, until radiative-convective equilibrium (RCE) is achieved. In order to minimize computational expense and storage, Lagrangian particles are not used in this phase. Then, I restart the model with the LPDM and run it for 12 h with data collected every minute of model time. I consider this as the *control run*. Horizontal and temporal averages of temperature and relative humidity with respect to liquid water during this interval are shown in Figure 1.

Whenever the temperature within a grid box containing graupel is above freezing, melting occurs, and the microphysics scheme of SAMiso determines the fraction of graupel to be converted to liquid water. If, in addition, the grid box is unsaturated with respect to water, SAMiso also computes how much liquid

water evaporates from the partially melted graupel hydrometeors (Blossey et al., 2010; Chen & Sun, 2002; Pruppacher & Klett, 2010). This process is a source of water vapor in downdrafts and, because evaporation generally causes fractionation of water isotopologues, it could also alter the isotopic abundances of downdraft or cold pool water vapor. In order to test the impact of this fractionation process, I also run a sensitivity experiment, in which the evaporation of partially melted graupel is deactivated. The sensitivity experiment is conducted with the same configuration and spin up technique as the control run but without the LPDM.

2.2. Definitions

In this work, I focus on three stable water isotopologues: the lightest, and more abundant, $H_2^{16}O$, and the heavier $H_2^{18}O$ and HDO. For simplicity, I will omit the word "stable" for the remainder of this manuscript, and, when possible, I will denote the heavier water isotopologues by the atomic isotopes (e.g., ^{18}O in lieu of $H_2^{18}O$). I also adhere to the general convention of denoting ratios of a heavier isotope $\aleph \in \{^{18}O, D\}$ to the lighter isotope as:

$$R_{\aleph} = \frac{q_{\aleph}}{q_v} \tag{2}$$

where $q_{\aleph}$ represents the mixing ratio of the heavier isotope $\aleph$, and q_v that of the lighter isotope. The abundance of a heavy isotope will be denoted by:

$$\delta\aleph = \left(\frac{R_{\aleph}}{R_{\mathrm{VSMOW}}} - 1\right) \times 1000, \tag{3}$$

where R_{VSMOW} is the International Atomic Energy Agency (IAEA) Vienna Standard Mean Ocean Water (VSMOW) standard (Araguás-Araguás et al., 2000). For simplicity, for the remainder of the manuscript, every isotope ratio $R_{\aleph}$ will be normalized by R_{VSMOW} for the particular isotope under consideration.

The Lagrangian derivative for $\ln(R_{\aleph})$ can be written as:

$$\frac{1}{R_{\aleph}}\frac{DR_{\aleph}}{Dt} = \frac{1}{q_{\aleph}}\frac{Dq_{\aleph}}{Dt} - \frac{1}{q_v}\frac{Dq_v}{Dt}, \tag{4}$$

Estimating the Lagrangian derivatives of $q_{\aleph}$ and q_v using the LPDM as described in Equation 1, the above equation becomes:

$$\frac{1}{R_{\aleph}}\frac{DR_{\aleph}}{Dt} = \sum_i \left[\frac{\left(\dot{q}_{\aleph}\right)_i}{q_{\aleph}} - \frac{\left(\dot{q}_v\right)_i}{q_v}\right], \tag{5}$$

where $i \in \{mic, dif, mix\}$. Equation 5 suggests that, from a Lagrangian perspective, the fractional change of the isotope ratio $R_{\aleph}$, or the change of $\ln(R_{\aleph})$, in a time step can be computed as a sum of three terms due to different physical processes, each of which can be determined with the use of the LPDM.

I define the *subcloud layer* as the portion of the model domain that includes the surface and in which the time- and domain-averaged non-precipitating total water mixing ratio, q_n, is below 10^{-5} g kg^{-1}. The latter is defined as the sum of cloud liquid water and cloud ice mixing ratios. With the settings described above, this corresponds to the bottom 631 m, approximately 70 hPa, of the model domain.

Cold pools are identified using a Lagrangian tracking algorithm (Torri et al., 2015; Torri & Kuang, 2016b, 2019). Grid boxes in the subcloud layer for which the density potential temperature anomaly with respect to the horizontal mean, θ'_{ρ}, is lower than −1 K, and in which the precipitating total water mixing ratio, q_p, is greater than 0.3 g kg^{-1} are flagged. The latter variable is defined as the sum of rain, snow, and graupel mixing ratios. Each cluster of flagged grid boxes is then considered in a four-dimensional space which also includes the time direction. If the cluster contains more than 250 grid boxes, it is given a unique identification number. I refer to these types of clusters as *cold pool cores*. Finally, each Lagrangian particle that enteres a cold pool core is assigned the same identification number, which is carried until the particle is in a grid box

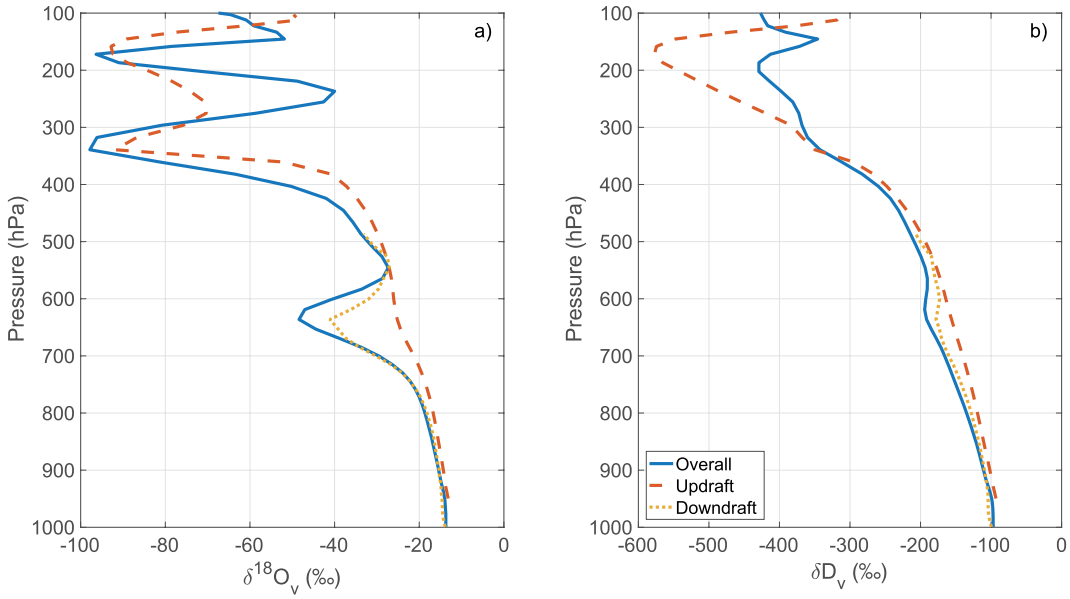

Figure 2. Average vertical profiles of $\delta^{18}O_v$ (a) and δD_v (b) for the environment (solid blue line), downdrafts (dotted yellow line), and updrafts (dashed red line).

where θ'_ρ is equal or greater than zero. Because a number of thresholds were introduced in the algorithm, I tested the sensitivity of the results by modifying each of the thresholds, but there was no qualitative change.

Following Torri and Kuang (2016b), I use a probability distribution function approach and define as *moist patches* those grid boxes at or above the 90th percentile of the distribution of q_v in the subcloud layer.

I also consider only those *downdrafts* that penetrate into the subcloud layer and inject air to form a cold pool (Torri & Kuang, 2016a). These are identified by selecting the Lagrangian particles that are found inside of cold pool cores and by tracking them back in time until the moment when they acquired negative velocity. The height from where the particle starts descending is called the *initial height* (Torri & Kuang, 2016a).

Finally, *updrafts* are identified in the following way. Whenever a particle is in a grid box that has a positive vertical velocity greater than 0.5 m s^{-1} and q_n greater than 0.1 g kg^{-1}, it is flagged. If these conditions are maintained for at least 5 min, the particle is followed until either condition is violated consistently for 5 min.

3. Results

3.1. An Overview

In order to better understand some of the features observed in the subcloud layer, this section begins with a brief overview of the vertical profiles of isotope abundances. The solid blue curves in Figure 2 show the values of $\delta^{18}O_v$ (a) and δD_v (b) averaged over the horizontal directions and time.

Both curves show a minimum at 200 hPa and an enrichment at higher levels, which is consistent with previous studies (e.g., Blossey et al., 2010; Bony et al., 2008; Hanisco et al., 2007; Kuang et al., 2003; Webster & Heymsfield, 2003). The solid blue curve on the left plot contains two additional minima, one at approximately 640 hPa and one at 340 hPa. At these heights, the vertical profile of δD_v also shows a decrease, albeit less marked than that of $\delta^{18}O_v$. The profile of $\delta^{18}O_v$ averaged only over the updrafts, denoted by the dashed red curve, also exhibits a marked minimum in the upper troposphere. I hypothesize that the minimum in the upper troposphere is due to vapor deposition on cloud ice and snow. This is consistent with Figure 3a, which shows the vertical profiles of the abundances of $\delta^{18}O$ in the hydrometeor species predicted by the microphysics scheme for the control run. In the plot, the solid red and the dashed purple curves correspond to the $\delta^{18}O$ of cloud ice and snow, respectively, and they both show very enriched values in the upper troposphere, in the layer where the vapor has a minimum.

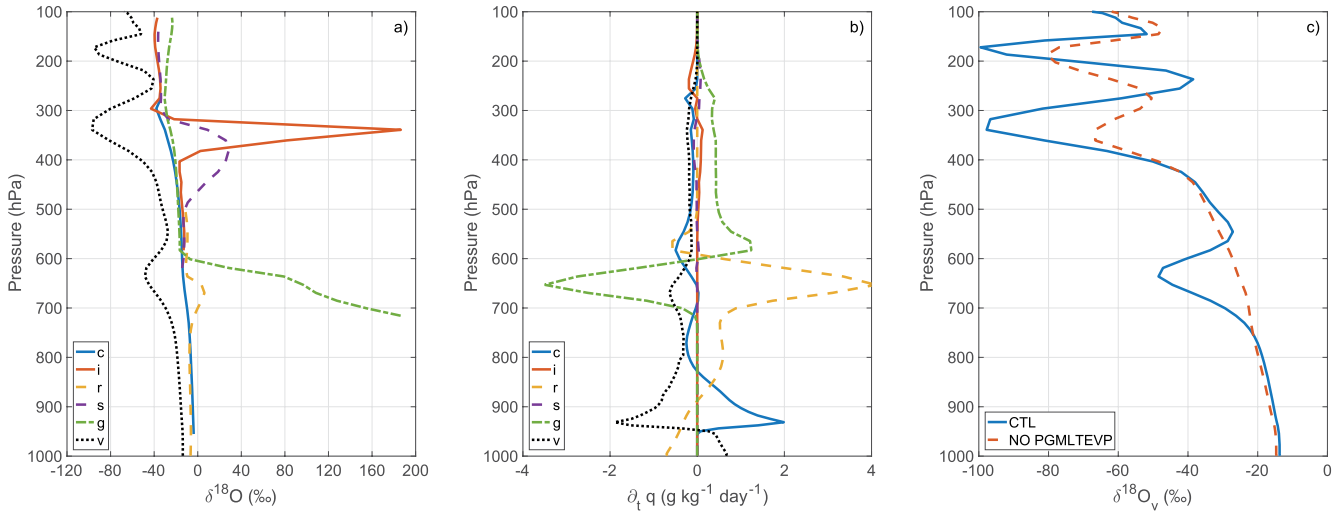

Figure 3. (a) Vertical profiles of $\delta^{18}O$ for cloud liquid water (solid blue), cloud ice (solid red), rain (dashed yellow), snow (dashed purple), graupel (dash-dotted green), and water vapor (dotted black). (b) Vertical profiles of microphysical tendencies for hydrometeors (colors as in left panel). (c) Comparison between the vertical profile of $\delta^{18}O_v$ in the control run (solid blue) and in the sensitivity run with no evaporation of partially melted graupel (dashed red).

Figure 3b also shows that at approximately 650 hPa graupel appears to melt into rain. By itself, this process does not cause fractionation, but some of the partially melted graupel eventually evaporates. I hypothesize that this is the reason behind the mid-tropospheric minimum in $\delta^{18}O_v$ seen in Figure 2a, which is also consistent with the fact that the updraft water vapor does not show a similar feature, while the downdraft (dotted yellow curve) does. In order to test this hypothesis, Figure 3c shows a comparison between $\delta^{18}O_v$ in the control (solid blue) and in the sensitivity experiment described in Section 2, where evaporation of partially melted graupel is not allowed to happen (dashed red). In the latter case, the mid-tropospheric minimum has disappeared.

As mentioned above, the vertical profile of δD_v also shows a decrease at 650 hPa, albeit not as strong as the one seen in $\delta^{18}O_v$. This is likely a result of small differences in the molecular weights and, in turn, vapor pressures, of the heavier isotopologues which make HDO evaporate more easily than $H_2^{18}O$. Because of this, hydrometeors experiencing evaporation become relatively more enriched—and, correspondingly, the vapor more depleted—in $H_2^{18}O$ than in HDO.

3.2. The Isotopic Composition of Downdrafts

In order to understand the initial isotopic composition of cold pools, this section begins by examining the composition of the precipitation-driven downdrafts that are responsible for generating cold pools. I first present results obtained using Lagrangian particles, and then I discuss a consistency check based on a bulk downdraft model.

3.2.1. Results From the LPDM

Following the definitions introduced in Section 2.2, I select all the downdraft particles and examine their history, from the moment when they enter the downdraft until they arrive in a cold pool core.

Figure 4 shows the contributions, averaged over all the downdraft particles, to the right-hand side of Equation 5 due to microphysical processes (a) and to mixing (b). The former include rain evaporation and vapor-liquid exchanges often referred to as equilibration effects (e.g., Graf et al., 2019). The results are shown as a function of pressure and time since the particles' entrance in the downdraft. Above the surface, the contributions due to diffusion are much smaller than the other two terms and are not shown. The figure only shows results for deuterium, whereas those for oxygen-18, shown in Figure S1, look qualitatively similar.

Between 850 hPa and 950 hPa, evaporation and equilibration tend to have an overall depleting effect on the vapor in the downdraft. Due to differences in vapor pressures, heavier isotopes tend to accumulate

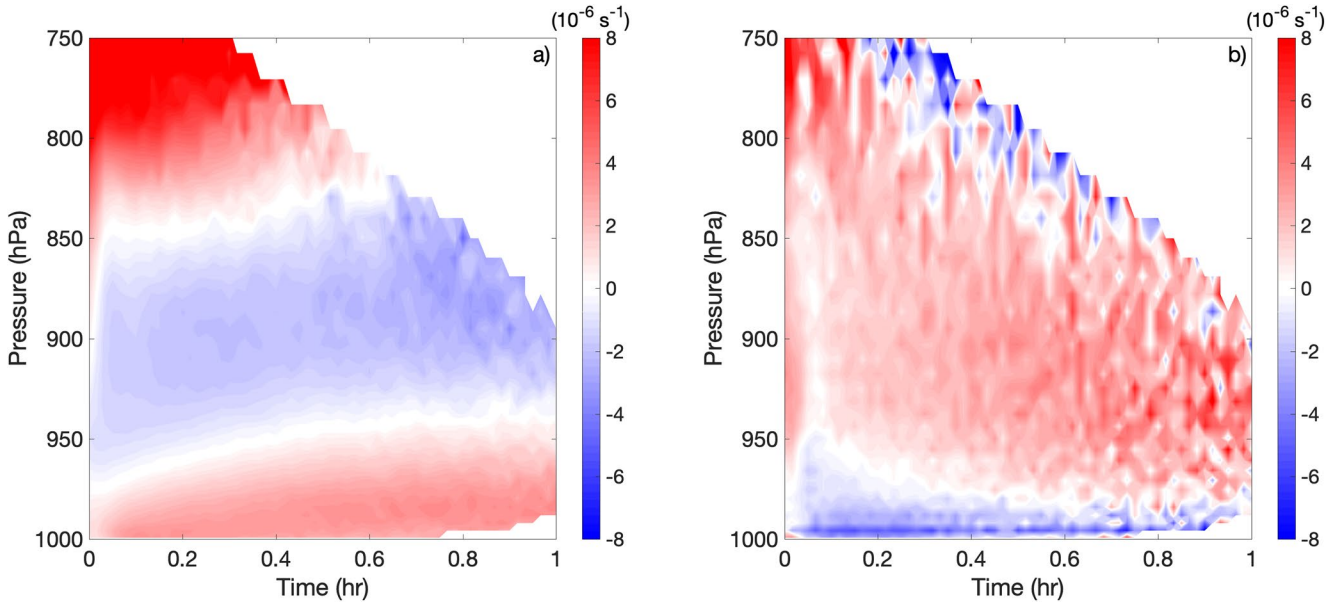

Figure 4. Contributions to Equation 5 due to microphysical processes (a) and mixing (b) for downdrafts.

preferentially in the liquid phase while droplets fall in the downdraft, thus creating progressively more enriched hydrometeors and depleted vapor. As the fall in the downdraft continues, however, some of the droplets eventually evaporate completely, releasing heavier isotopes. This might explain why evaporation tends to have an enriching effect below 950 hPa, in the subcloud layer, although equilibrium fractionation may also play an important role (e.g., Aemisegger et al., 2015; Graf et al., 2019; Lee & Fung, 2008; Risi et al., 2020). The positive values above the 800 hPa level are likely due to the fact that both rain and partially melted graupel tend to be relatively enriched between 600 hPa and 750 hPa (see Figure 3a), so that their evaporation would also enrich the vapor.

Mixing has an overall enriching effect. In Figure 2, the vertical profile of isotope abundances in the vapor decreases monotonically approximately up to an altitude of 640 hPa. Thus, a particle in a downdraft is surrounded by progressively more enriched vapor as it descends toward the surface. The figure also suggests that the contribution due to mixing increases with time, although this could simply be due to the fact that downdrafts become more depleted with time (not shown). In addition, this effect could also be partly attributed to a sampling bias, given that progressively fewer particles are found for increasing values of time that they spent in the downdraft.

3.2.2. Consistency Check With a Bulk Model

I test the consistency of the results presented above with a downdraft model similar to the bulk plume models used to study shallow cumulus clouds (e.g., Siebesma & Cuijpers, 1995; Siebesma et al., 2020). I begin with the assumption that the bulk downdraft can be separated from its surrounding environment. In particular, I consider as part of a downdraft any grid box for which $w < -0.5$ m s^{-1} and $q_p > 0.3$ g kg^{-1}. The requirement for q_p is particularly useful for minimizing the risk of including gravity waves in the category. Assuming the hydrostatic approximation and steady conditions, the bulk equation for water vapor mixing ratio in the simple model can be written as:

$$\partial_p q_v = \epsilon_p \left(\overline{q}_v - q_v \right) + \frac{E_v}{g M_{dn}}, \tag{6}$$

where ϵ_p is the entrainment coefficient in pressure coordinates, g the gravitational acceleration, E_v is the horizontally averaged evaporation rate associated with q_v, and I define $M_{dn} = a_{dn}\omega/g$ as the downdraft mass flux, a_{dn} being the fractional area coverage of downdrafts. The entrainment coefficient, ϵ_p, can be diagnosed from the equation for moist static energy, h:

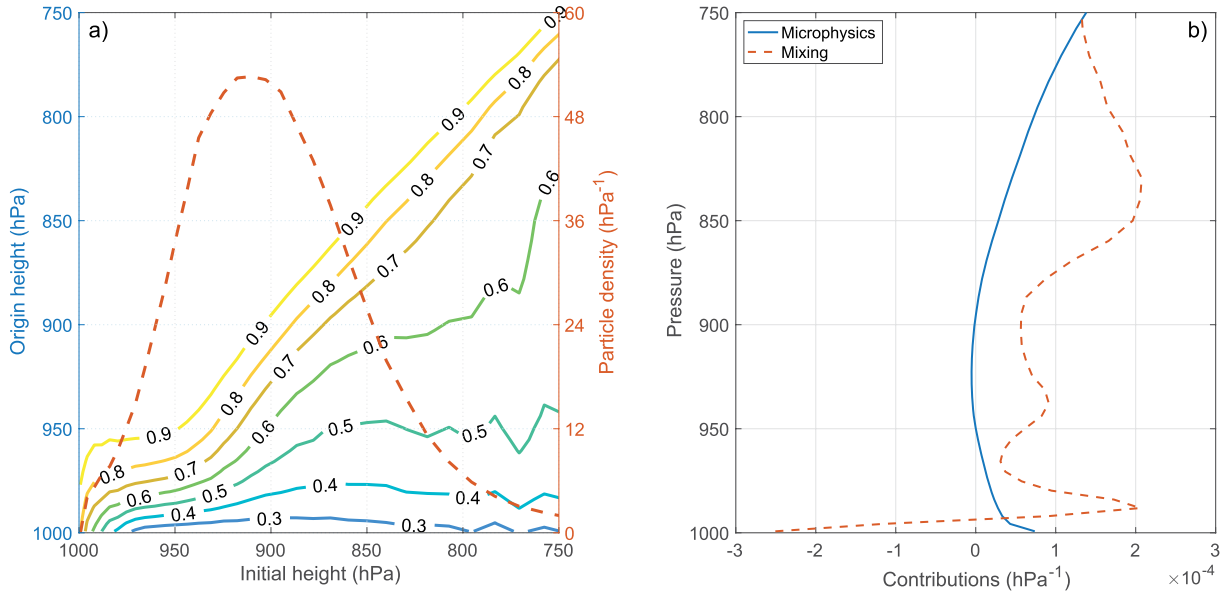

Figure 5. (a) Isolines for the cumulative distribution function of the origin height (y-axis) of downdraft particles as a function of their initial heights (x-axis); the red dashed line represents the downdraft particle density as a function of the particles' initial heights. (b) Contributions to Equation 9 due to microphysical processes (solid blue) and entrainment (dashed red) for deuterium isotopes.

$$\epsilon_p = \frac{\partial_p h}{\left(\overline{h} - h\right)}, \tag{7}$$

where h is the moist static energy of the downdraft, and $\overline{h}$ that of the environment. Both are diagnosed from the model output by taking horizontal averages at every level.

The mixing ratio of a heavier isotope follows a similar formula to Equation 6. Using the definition of $R_\aleph$, the equation for $q_\aleph$ can be written as:

$$\partial_p\left(R_\aleph q_v\right) = \epsilon_p\left(\overline{R_\aleph q_v} - R_\aleph q_v\right) + \frac{E_\aleph}{gM_{dn}}, \tag{8}$$

where $E_\aleph$ is the horizontally averaged evaporation rate associated with $q_\aleph$. Subtracting $R_\aleph$×Equation 6 from Equation 8, and after having verified that $\overline{R_\aleph q_v} \approx \overline{R}_\aleph \overline{q}_v$ (not shown):

$$\frac{\partial_p R_\aleph}{R_\aleph} = \frac{\epsilon_p \overline{q}_v}{q_v}\left(\frac{\overline{R}_\aleph}{R_\aleph} - 1\right) + \frac{1}{gq_v M_{dn}}\left(\frac{E_\aleph}{R_\aleph} - E_v\right), \tag{9}$$

where the left term in the right-hand side is the contribution due to entrainment, and the rightmost term is the contribution due to microphysical processes. In the above equation, the terms q_v and $R_\aleph$ are computed by taking the horizontal averages at every level over downdraft grid boxes. Equations 9 and 5 can be directly compared by writing the Lagrangian derivative in explicit form and assuming a steady state.

Finally, estimates of $\overline{q}_v$ and $\overline{R}_\aleph$ are needed to compute the terms on the right-hand side of Equation 9. The colored lines in Figure 5a show the cumulative distribution of origin heights, defined as the height that a particle has 60 min prior to its entrance in a downdraft, as a function of the particles' initial heights. The latter, introduced in Section 2.2, is defined as the height of the particle when it enters the downdraft and only for for those particles that are eventually found inside a cold pool core. Most of the particles that begin their descent above 950 hPa originate in the subcloud layer, and only approximately 30% originate near their initial height. The vast majority of the particles originating in the subcloud layer ascend in an updraft until they acquire negative buoyancy and start descending (Torri & Kuang, 2016a). In the case of particles

descending from greater heights, a larger portion originates at the particle's initial height, although these constitute only a small fraction of the downdraft. For simplicity, I assume that $\overline{q}_v$ and $\overline{R}_N$ are a weighted average between the mean updraft values (70%) and the environment values (30%) at a particular height. I tested the sensitivity of the results to this choice by varying the proportions by 5% in both directions but did not notice significant changes.

The contributions to Equation 9 due to entrainment and microphysics are represented respectively by the dashed red and the solid blue curves in Figure 5b. Qualitatively, the curves seem to confirm the conclusions derived from Figure 4, with evaporation and equilibration acting to deplete the downdraft between 900 and 950 hPa and enrich it elsewhere, and mixing having an overall enriching effect.

3.3. The Isotopic Composition of Cold Pools

After having examined which processes affect the isotopic composition of downdrafts, in this section I continue the analysis and focus on cold pools. I begin by discussing the cold pool initial isotopic composition, then I present results obtained using Lagrangian particles on which processes affect water vapor isotopes as cold pools propagate. Finally, I show a consistency check based on a simple axisymmetric cold pool model.

3.3.1. Positive $\delta^{18}O_v$ Anomalies in Cold Pool Cores

Figures 6a and 6b show snapshots of the near-surface values of $\delta^{18}O_v$ and δD_v in the control run. The figures show that cold pools tend to be associated with more depleted water vapor compared to other areas in the domain, particularly in their cores. This is likely due to the fact that the air injected in cold pools originates in the free troposphere and also that vertical profiles of water vapor heavy isotope abundances generally decrease with height, as shown in Figure 2.

Figure 6a shows the presence of relatively enriched values of $\delta^{18}O_v$ in the coldest regions of some cold pools. A more systematic representation of this can be found in Figure 7a, which shows the joint probability density function of near-surface values of $\delta^{18}O_v$ and θ'_ρ in the control run. The presence of an upper lobe for θ'_ρ between -1 K and -2.5 K confirms the existence of relatively enriched values in cold regions of some cold pools.

I hypothesize that these anomalies are related to the evaporation of partially melted graupel that takes place in the mid-troposphere. The fractionation that happens during this process makes hydrometeors progressively more enriched. As they fall through the atmosphere, some of the hydrometeors eventually evaporate completely, thus enriching the vapor where the process takes place.

In order to test the consistency of this hypothesis, I construct a similar joint probability density function to the one shown in Figure 7a, but for the sensitivity experiment where evaporation of partially melted graupel was turned off. The result, presented in Figure 7b, shows no values above approximately -13‰, which is consistent with the hypothesis. Finally, differences in molecular weights between the heavier isotopes are likely the reason why there are no δD_v-enriched areas in cold pool cores. The slightly lighter HDO molecules evaporate more easily than $H_2^{18}O$, and therefore accumulate less in hydrometeors as they fall and evaporate. Thus, when the hydrometeors evaporate completely, they enrich the water vapor with $H_2^{18}O$ isotopes more than with HDO.

3.3.2. Results From the LPDM

After having focused on the initial isotopic composition of cold pool water vapor, I now focus on the propagation stage and quantify the relative roles played by the surface latent heat fluxes and entrainment in modulating cold pool isotopic composition.

Figures 6c and 6d show the near-surface values of δD_v and $\delta^{18}O_v$, respectively, averaged over all the cold pools detected by the tracking algorithm discussed in Section 2, presented as a function of cold pool radius and age. Notice that the color bars of these figures cover a relatively smaller range of values than those in the top panels of the same figure. Slight differences between cold pools and the histories they experience are likely responsible for this.

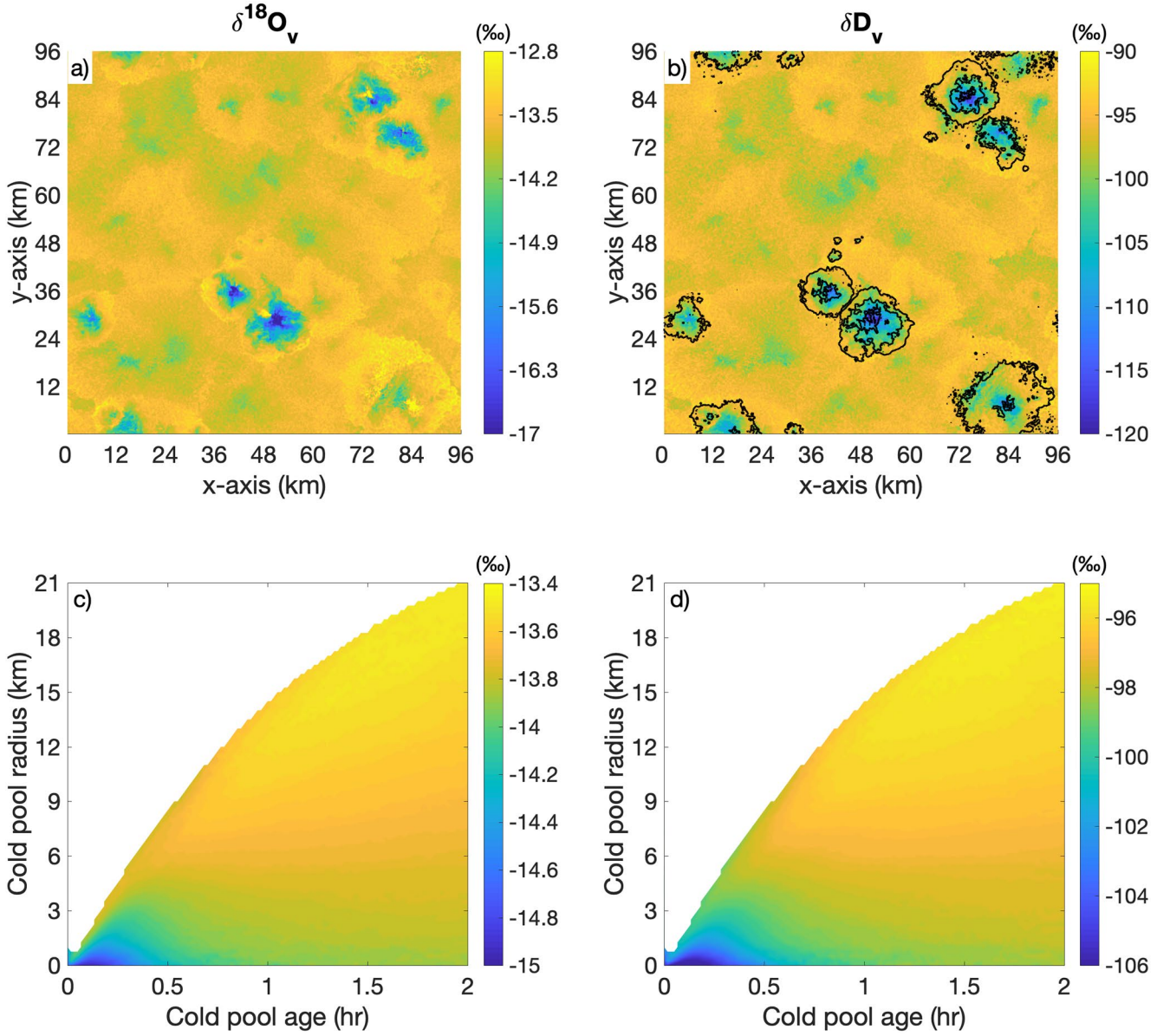

Figure 6. Top: Snapshots of near-surface values of $\delta^{18}O_v$ (a) and δD_v (b); the black contours represent negative anomalies of θ_ρ at −1 K intervals starting from −0.25 K. Bottom: Near-surface values of $\delta^{18}O_v$ (c) and δD_v (d) averaged over all the detected cold pools and shown as a function of cold pool radius and age.

During its first half hour of life, the cold pool gust front, which is the outer edge of the cold pool, propagates with the greatest speed. This can be appreciated simply by looking at how rapidly the values of the maximum cold pool radius grow initially. This is the phase during which the downdraft is injecting air in the subcloud layer. Particles near the gust front become almost as isotopically enriched as their surrounding environment. In the following stages, after the end of the precipitation-driven downdraft that originated it, the cold pool propagation begins to slow and its properties change at a slower pace.

In order to quantify the role played by different physical processes (e.g., microphysics, surface latent heat fluxes, and entrainment), I follow a similar approach to the one adopted in Section 3.2. For each Lagrangian particle at any height in a tracked cold pool, I save the tendencies the particle experiences due to mixing, diffusion, and microphysics for every time step and for each water vapor isotope. Then, I use Equation 5 to quantify how much each process contributes to changes in the isotopic ratio. The results for diffusion and mixing are shown in Figures 8a and 8b, respectively, as a function of the radius and the age of the cold pool.

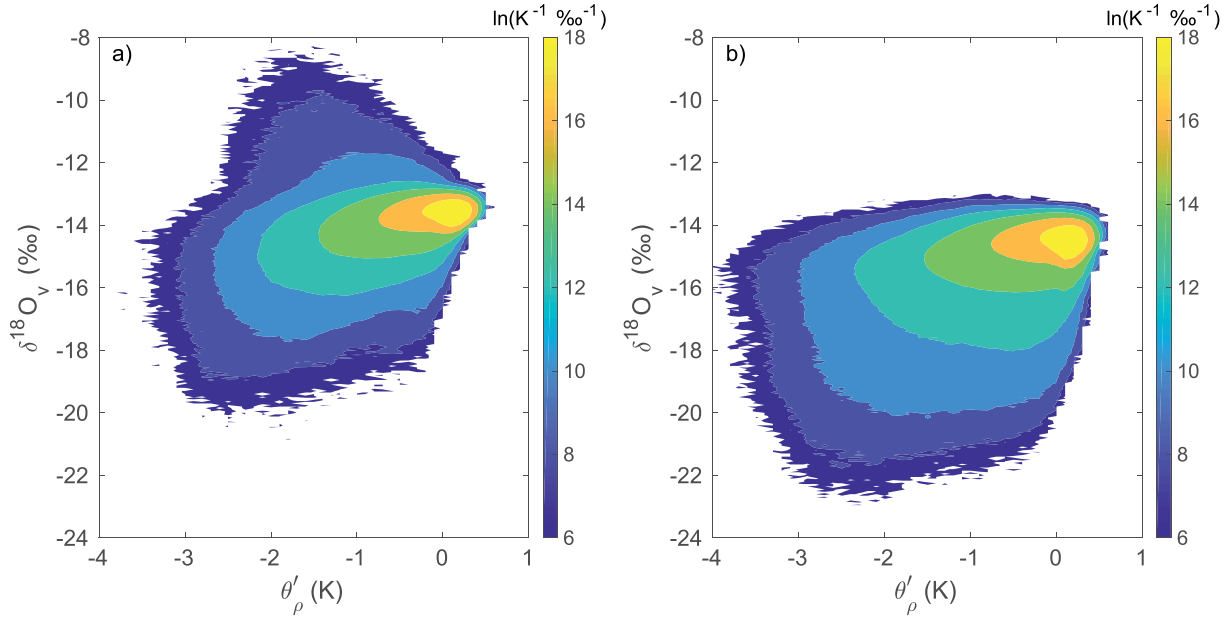

Figure 7. Logarithms of the joint distributions of near-surface values of $\delta^{18}O_v$ and θ'_ρ for the control run (a) and for the sensitivity run where the evaporation of partially melted graupel is turned off (b).

The contributions due to microphysics are negligible and are not shown here. The figures only show the contributions for $\ln(R_D)$, whereas those for $\ln(R_{18_O})$ are shown in Figure S2, and look qualitatively similar.

The diffusion term, which is related to surface latent heat fluxes, is larger than the mixing term across the entire cold pool life cycle and at all radii. The contribution is greatest during the initial stage of cold pool propagation, which roughly corresponds to the first 30 min of its life cycle. This is likely the main process responsible for the rapid enrichment of cold pool water vapor isotopes noticed a few paragraphs above.

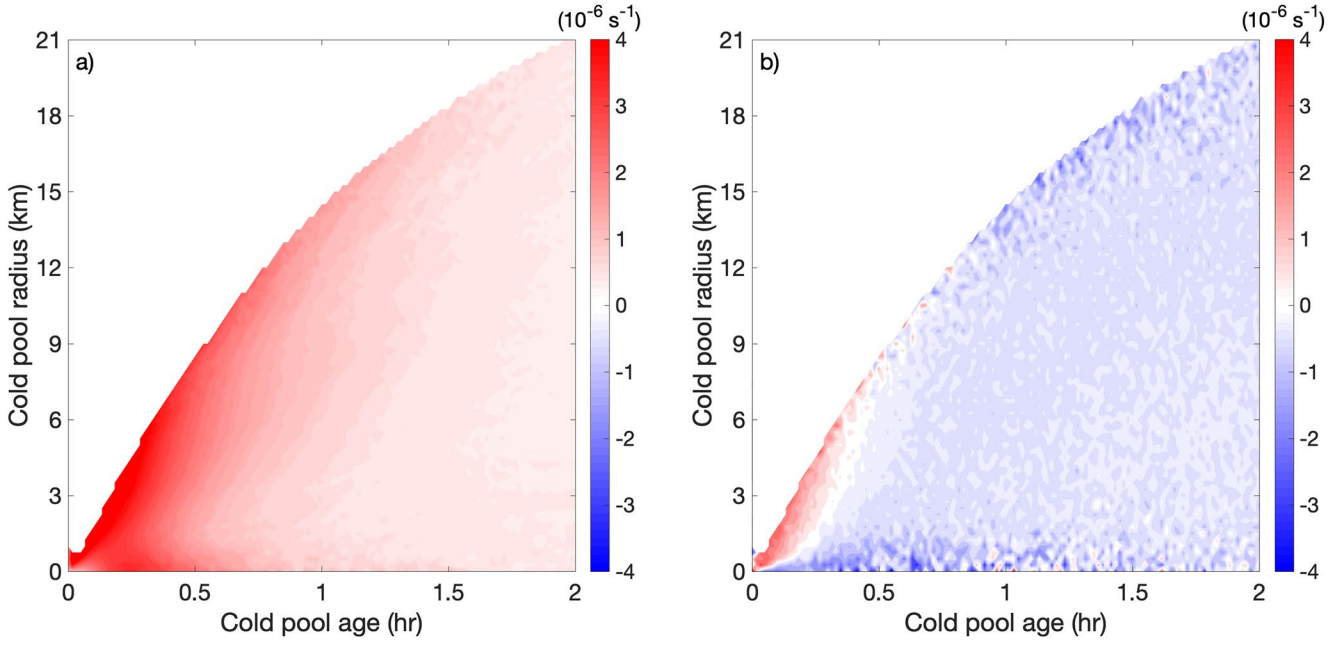

Figure 8. Contributions to changes of $\ln(R_D)$ for Lagrangian particles in cold pools due to diffusion (a) and mixing (b) shown as a function of cold pool radius and age.

The term decreases after approximately an hour following the birth of the cold pool, but it always remains greater than the mixing term.

The mixing term is positive at outer radii at the very beginning of the cold pool life cycle but is negative at all other times and radii. A more careful look at the data shows that the values at the cold pool gust front are greater in magnitude than those in the rest of the cold pool approximately by a factor of 2. This is reasonable considering how depleted cold pool cores are with respect to their surrounding environment.

As for the negative values afterward, these are likely due to two reasons. The first is that, during the mature stage, cold pool gust fronts become anomalously rich in heavy isotopes compared to the environment, as can be seen in the top panels of Figure 6. Entrainment of subcloud layer air during this stage would necessarily deplete the water vapor. Furthermore, it has been shown that cold pools experience a large number of collisions with other cold pools during their life cycle (Torri & Kuang, 2019). Because cold pools are particularly depleted during the initial stages of their life cycle, the collision of a mature cold pool with a younger one would have a depleting effect on the former.

3.3.3. Consistency Check With an Axisymmetric Cold Pool Model

I test the consistency of the LPDM results presented above by using a simple cold pool model. To construct this model, I assume that cold pools are axisymmetric throughout their life cycle and that they are well-mixed in the vertical direction. With these assumptions, I use a system of shallow-water equations to describe the evolution of the cold pool and its properties (see e.g., Ross et al., 2004, 2006; Ungarish, 2009). For simplicity, I also assume that the reference state is in hydrostatic balance, that the cold pool satisfies the Boussinesq approximation and, in addition, that there is no detrainment from the cold pool. If $h(r, t)$ is the height of the cold pool from the surface in pressure coordinates and $u_r(r, t)$ its radial velocity, then:

$$\partial_t h + r^{-1}\partial_r\left(r u_r h\right) = \omega_e, \tag{10}$$

$$\partial_t(h q_v) + r^{-1}\partial_r\left(r u_r h q_v\right) - \omega_e \overline{q_v} = g L_v^{-1} F_v \tag{11}$$

ω_e is the entrainment pressure velocity, g is the gravitational acceleration, L_v is the latent heat of vaporization, F_v is the latent heat flux, q_v is the water vapor mixing ratio of cold pool air, and $\overline{q_v}$ is the mixing ratio of the air entrained. Using the product rule of derivation, and subtracting the above equations, I obtain:

$$\partial_t q_v + u_r \partial_r q_v = h^{-1}\left[g L_v^{-1} F_v + \omega_e\left(\overline{q_v} - q_v\right)\right]. \tag{12}$$

The two terms on the right-hand side are due to surface latent heat fluxes and entrainment of air from the subcloud layer. Given that a similar equation applies to $q_\aleph$, and considering the definition of $R_\aleph$, I proceed in a similar way to Section 3.2 and obtain:

$$\frac{1}{R_\aleph}\left(\partial_t R_\aleph + u_r \partial_r R_\aleph\right) = \frac{1}{h}\left[\frac{g}{L_v q_v}\left(\frac{F_\aleph}{R_\aleph} - F_v\right) + \omega_e \frac{\overline{q_v}}{q_v}\left(\frac{\overline{R_\aleph}}{R_\aleph} - 1\right)\right], \tag{13}$$

where $\overline{R_\aleph}$ is the isotope ratio in the environment. The above equation provides a way to distinguish the contributions to the changes in $R_\aleph$ of the expanding cold pool due to surface fluxes and those from entrainment of subcloud air. All the terms written in Equation 13 can be diagnosed from SAMiso output, using the cold pool tracking algorithm to classify the data according to the distance from the cold pool center and the time since the birth of the cold pool that a grid box is part of.

Because of the turbulent nature of cold pools, and given that there is no real discontinuity that separates a cold pool from its surrounding environment, there is no single method to determine the height of a cold pool. Here, I define $h(r, t)$ as the average pressure height from the surface of cold pool particles at a given point in time and space:

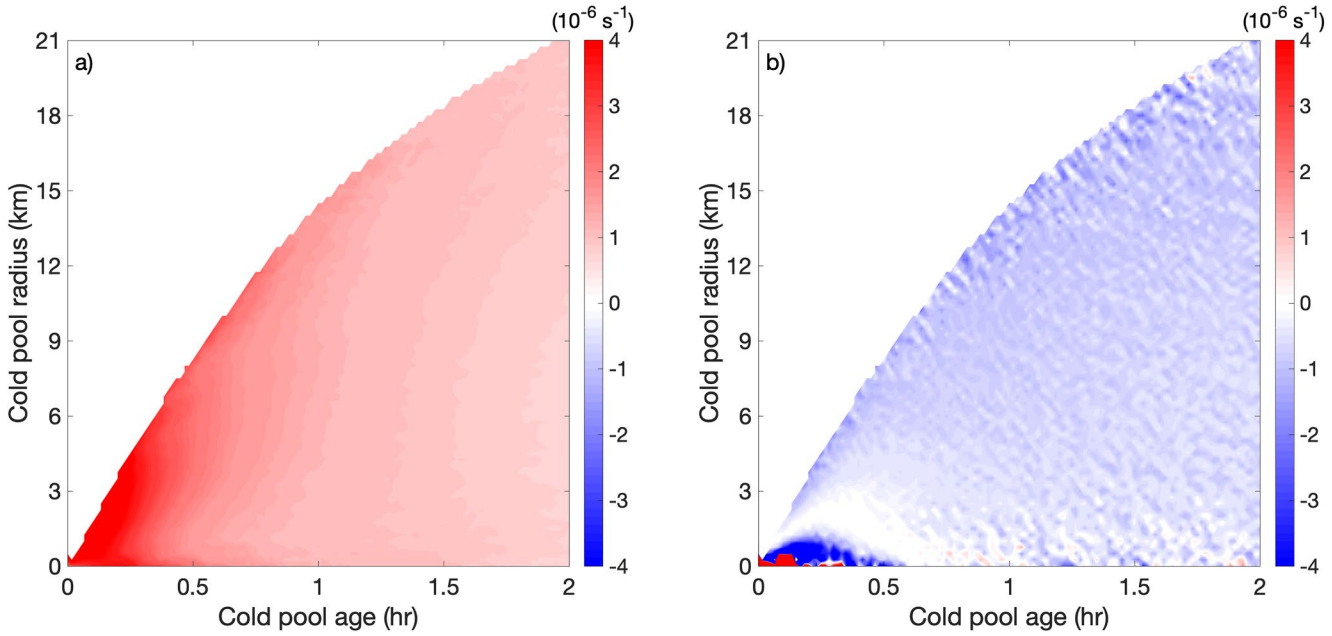

Figure 9. Contributions to Equation 13 due to surface latent heat fluxes (a) and entrainment (b) shown as a function of cold pool radius and age.

$$h(r,t) = N(r,t)^{-1} \int_{p_s}^{p_t} \left(p_s - p\right) n(r,p,t)\, dp, \tag{14}$$

$$N(r,t) = \int_{p_s}^{p_t} n(r,p,t)\, dp, \tag{15}$$

where $n(r, p, t)$ is the density of particles at a given point in the cold pool, and p_t and p_s are the values of pressure at the top and at the surface of the domain, respectively. I conducted sensitivity tests where cold pool height was defined as the height of the 75th and 90th percentile of $n(r, p, t)$ and I noticed no qualitative differences. Finally, $\overline{q_v}$ and $\overline{R_N}$ are computed by averaging the variables in the top 25 hPa of the subcloud layer, and the entrainment pressure velocity is diagnosed using Equation 12.

Figures 9a and 9b represent, respectively, the contributions from the latent heat flux and the entrainment terms of Equation 13. The figures represent the results for deuterium, but those for oxygen-18 are qualitatively similar. Overall, there is good agreement with the results shown in Figure 8, which were obtained by examining the histories of Lagrangian particles within cold pools. The flux term appears to be greater than the entrainment term and tends to enrich the cold pool water vapor. The entrainment term is relatively small in the body of the cold pool.

Unlike the results obtained with the LPDM, the entrainment term here seems to only have a depleting effect on the cold pool. However, I assumed that entrained air parcels originate in the upper portions of the subcloud layer, which are relatively more depleted than the surface layer or even mature cold pool gust fronts, where air may actually be originating in the simulation. These differences notwithstanding, the favorable comparison between the results obtained using different diagnostic techniques provides some confidence in the conclusions.

3.4. The Isotopic Composition of Moist Patches

In this section, I examine the isotopic composition of air parcels in moist patches, the anomalously moist areas surrounding cold pools. In particular, I present some results that show that isotopes could potentially be used to diagnose the origin of the water vapor found in the patches. This is an area where there is still some controversy, with some modeling studies suggesting that rain evaporation plays a particularly important

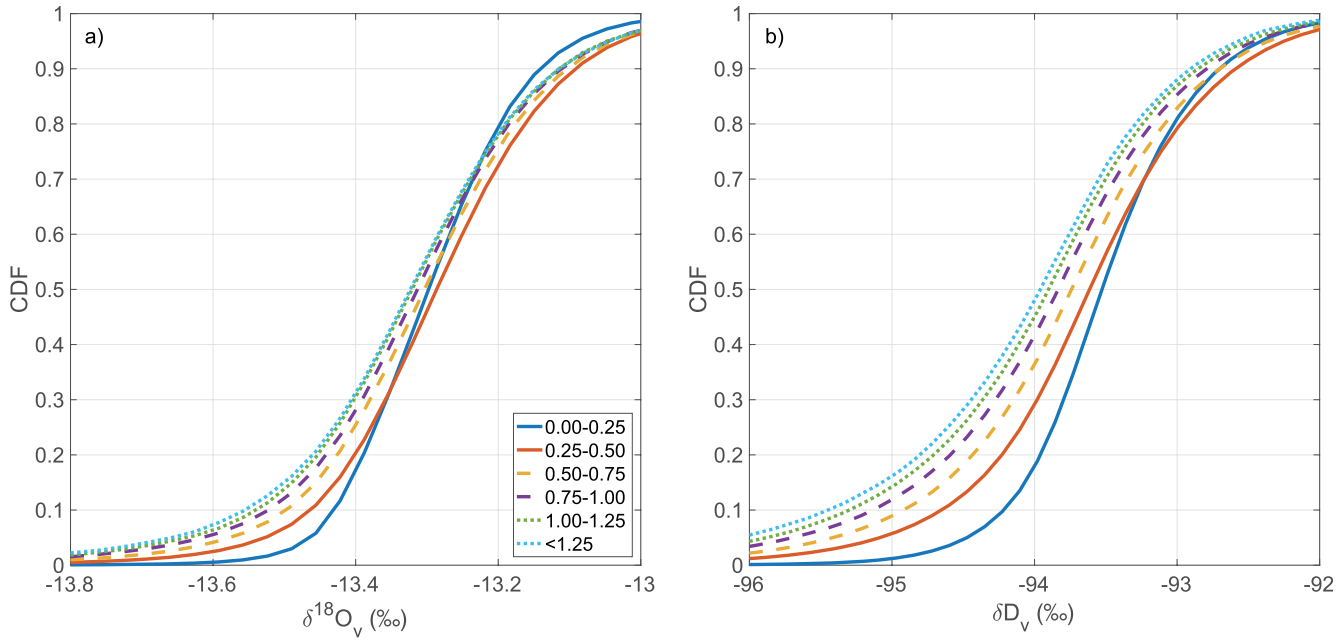

Figure 10. Cumulative distribution functions of $\delta^{18}O_v$ (a) and δD_v (b) for particles in cold pool moist patches grouped by r_e.

role in generating moist patches (Seifert & Heus, 2013; Tompkins, 2001; Torri & Kuang, 2016b), while others suggest that surface latent heat fluxes are the main responsible instead (Langhans & Romps, 2015; Schlemmer & Hohenegger, 2016).

Because rain evaporation has a depleting effect, at least above the boundary layer, and, as shown in Section 3.3, surface latent heat fluxes enrich water vapor, the isotopic composition of parcels in moist patches could vary according to how much water vapor was accumulated from either sources. Using the LPDM, whenever a particle is found in a moist patch grid box, I save its isotopic composition and examine its history in the previous 4 h. Finally, I group particles according to r_e, the ratio of water vapor accumulated through rain evaporation over that accumulated through surface latent heat fluxes. Because mixing also affects the isotopic composition of an air parcel, I have tried to further group the results by the ratio of water vapor accumulated through mixing to that accumulated through surface fluxes, but this did not cause any significant difference in the results. Furthermore, I have tested the sensitivity of the results to the choice of using a temporal window of 4 h by considering values of 3 and 6 h, but noticed no qualitative difference.

The panels of Figure 10 show the cumulative distribution functions for parcels in moist patches at the surface with different r_e as a function of their isotopic abundance at the time of collection. The lines in the different plots seem to confirm that particles that have accumulated more water vapor through rain evaporation rather than surface fluxes are generally more isotopically depleted. The curves appear relatively similar at higher values of isotopic abundances, but show some degree of divergence at lower values, with the curve for a higher r_e having a longer tail than that with $r_e = 0$.

A possible explanation for the lack of a larger spread among curves corresponding to different r_e values is that equilibration fractionation could account for a considerable portion of the microphysical effects experienced by downdraft parcels (e.g., Aemisegger et al., 2015; Graf et al., 2019). In this case, the contributions due to evaporation of rain and partially melted graupel would be relatively small and would not leave a particularly strong imprint in the isotopic composition of downdraft particles. If, on the other hand, evaporation was the leading factor in the microphysical changes, the opposing signs of the tendencies in Figure 4a could explain the lack of spread.

To further assess the role of microphysics, I compare the isotopic composition of Lagrangian particles when they exit a downdraft and enter a cold pool core with the hypothetical composition the particles would have had if microphysical processes had not caused isotopic fractionation. The latter is estimated

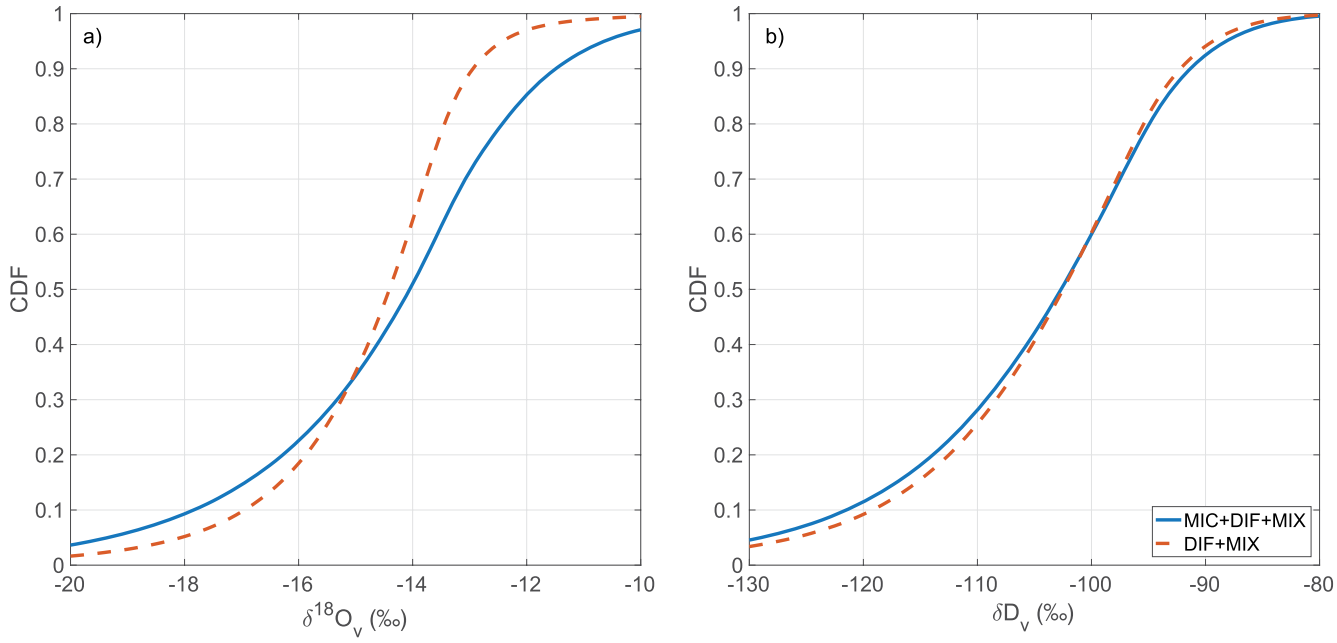

Figure 11. Cumulative distribution functions of $\delta^{18}O_v$ (a) and δD_v (b) abundances of downdraft particles when entering cold pool cores. The solid blue curves represent values reconstructed considering all processes, whereas the dashed red curves values obtained assuming that microphysical processes do not change the isotopic composition of particles. (See text for additional details).

by reconstructing the water vapor content of each particle as it descends in a downdraft, and adding to the particle the amount of heavier isotopes mixing ratios that would keep its isotopic composition unchanged. To determine the latter, I begin by assuming that, over a time step, microphysical processes make the water vapor mixing ratio of a particle in a downdraft change from q_v to $q_v + \delta q_v^e$ and the mixing ratios of heavier isotopes change from $q_\aleph$ to $q_\aleph + \delta q_\aleph^e$. By imposing that the isotope ratios at the successive time steps, $R_\aleph = q_\aleph/q_v$ and $R'_\aleph = (q_\aleph + \delta q_\aleph^e) / (q_v + \delta q_v^e)$, are equal, I obtain the following constraint on the heavy isotope mixing ratio added by evaporation:

$$\delta q_\aleph^e = R_\aleph \delta q_v^e. \tag{16}$$

Figure 11 shows the cumulative distribution function of isotopic abundances when particles reach the cold pool core. The solid blue curves refer to abundances reconstructed using the tendencies output from the model, whereas the dashed red curve denotes hypothetical abundances when microphysics does not cause fractionation. The results suggest that, because of the opposite trends above and below the boundary layer, microphysics appears to have an overall small impact on the median isotopic composition of downdraft particles when they enter a cold pool core.

4. Discussion

In spite of considerable progress over the last decade (see, e.g., Pincus et al., 2018; Siebesma et al., 2020, and references therein), many processes involved in cumulus convection remain underconstrained. In turn, this has repercussions on our understanding of the climate system, our ability to clarify its past, and predict its future. Although water vapor isotopes are useful tools in the study of climate, their application requires a comprehension of their behavior at a process-based level. Because numerical models used in this effort often do not explicitly resolve convection, however, many uncertainties remain.

In this study, I addressed some of these uncertainties by considering an idealized deep convective setting and focusing on cold pools, boundary layer features that are key ingredients of deep convective systems. I conducted the analysis with a combination of an Eulerian and a Lagrangian particle model, and I began by investigating the processes that influence the initial isotopic composition of cold pools. By analyzing

the history of the Lagrangian particles injected in the boundary layer by precipitation-driven downdrafts, I showed that mixing tends to enrich the isotopic composition of the particles throughout their descent (Figure 4). Microphysical processes, on the other hand, have contrasting effects: they deplete particles above the boundary layer and enrich them below. These results were confirmed using a bulk downdraft model as a consistency check. This model was constructed using many simplifying assumptions, but the favorable comparison with the results obtained using the LPDM provides some confidence in the conclusions reached using the latter.

I then examined the history of particles after they leave downdrafts and enter cold pools, and I determined the relative roles played by mixing and latent heat fluxes. Figure 8 shows that mixing has an enriching effect in the first moments of the cold pool life cycle, but otherwise it depletes cold pool water vapor. Given that cold pool collisions are relatively frequent (Feng et al., 2015; Drager & van den Heever, 2017; Torri & Kuang, 2019; Fournier & Haerter, 2019; Henneberg et al., 2020) and, as Figure 6 suggests, cold pools become more enriched as they mature, I attributed the initial enrichment caused by mixing to entrainment of old cold pool air parcels into the developing cold pool. Latent heat fluxes have an enriching effect that dominates the depletion due to mixing at all times. As a consistency check on these findings, I formulated an axisymmetric cold pool model based on shallow-water equations. Figure 9 shows good agreement with the results obtained using Lagrangian particles alone, discrepancies being likely due to the relative simplicity of the axisymmetric model used. Overall, the model confirms that latent heat fluxes are the primary responsible for the enrichment of cold pool water vapor isotopes.

These results could have important repercussions on our understanding of atmospheric water vapor isotopes. For example, while it is commonly assumed that downdrafts have an overall depleting effect on boundary layer isotopes (Kurita, 2013; Kurita et al., 2011; Risi et al., 2008, 2010), the findings in this work suggest that the role of downdrafts may depend considerably on the height at which they originate, with shallow downdrafts potentially having a neutral or even an enriching effect. Mixing could also counterbalance the role of microphysical processes by enriching the downdraft. These findings are consistent with, and could perhaps offer a process-based explanation to the results of Risi et al. (2020), who suggested that downdrafts are not one of the main factors that explains the amount effect as previously thought.

The fact that most of the contribution from surface latent heat fluxes to cold pool water vapor isotopes happens roughly within 30 min from the birth of the cold pool is also an interesting finding. While many budget models that have been constructed to understand boundary layer water vapor isotopes use an average value for the surface fluxes (e.g., Benetti et al., 2018; Galewsky et al., 2016; Risi et al., 2008, 2019), results presented here suggest that the variance of the fluxes should also be taken into account in the presence of cold pools.

The overall different effects that rain evaporation and surface fluxes have on water vapor were used in Section 3.4 to test whether vapor isotopes could help to constrain the origin of moist patches, a topic that is still a matter of debate (Chandra et al., 2018; Drager et al., 2020; Langhans & Romps, 2015; Li et al., 2014; Schlemmer & Hohenegger, 2016; Seifert & Heus, 2013; Torri & Kuang, 2016b; Tompkins, 2001). Indeed, Figure 10 suggests that particles in moist patches that have accumulated a greater fraction of water vapor through rain evaporation are more isotopically depleted than those that have accumulated more through surface latent heat fluxes. However, the differences between the curves are relatively small. For instance, the tenth percentile of the cumulative distribution functions differ at most by approximately 1.5‰ in δD_v, and the medians differ by roughly 0.5‰. Differences like these could be well below the standard errors associated with the observations, which would be problematic. However, there may be scenarios, for example with a drier free troposphere or with mesoscale organization, where downdrafts originate from greater heights, experience more rain evaporation and become, therefore, more depleted (Kurita, 2013; Kurita et al., 2011). In such cases, it might be possible that the differences between the isotopic compositions of particles in cold pool moist patches would be more significant, but I will leave a careful investigation of this for future studies.

Finally, as shown in Figure 6, cold pool cores in the control run often display $\delta^{18}O_v$-enriched areas, a feature that was attributed to the evaporation of partially melted graupel. This finding suggests that even observations of water vapor at the surface could reveal important details about microphysical processes happening in deep convective systems in the free troposphere. In turn, because not all microphysics schemes

parameterize the same processes in the same way, this constitutes also an example of how measurements of water vapor isotopes could be used to further constrain microphysics schemes used in numerical models.

While the results presented in this manuscript offer some insights on how downdrafts and cold pools affect atmospheric water vapor isotopes, there are some caveats due to the methodology followed. In particular, while single-moment microphysics schemes, such as the one used in this study, are computationally less expensive and relatively simpler than double-moment schemes, they do not perform as well as the latter (e.g., Igel et al., 2015). In terms of the main results of this work, a more sophisticated treatment of microphysical processes could have a direct impact on rain evaporation and, therefore, how this process affects the isotopic composition of downdrafts. However, this would not invalidate the conclusions of this study, but merely point to their sensitivity to external variables, such as evaporation rate, relative humidity, SST, and wind shear, just to cite few examples. An in-depth analysis of this sensitivity is the subject of ongoing work.

More generally, however, the fact that the results presented in this work were obtained only using numerical models certainly constitutes a limitation. While, on the one hand, this is not an uncommon practice, a comparison with observational data is always desirable, particularly as the inclusion of water isotopologues in numerical models is still relatively recent. The results discussed in this work will hopefully provide further motivation to conduct more observations.

5. Conclusions

In recent years, water vapor isotopes have attracted considerable attention as a means to constrain atmospheric processes that are particularly relevant in the climate system. In order to use this technique with confidence, however, an in-depth understanding of the behavior of atmospheric water vapor isotopes is required. This study contributes to this effort with a combination of an isotope-enabled cloud resolving model and a Lagrangian particle model, and by seeking a process-based understanding of water vapor isotopes in cold pools, which are key components of deep convective systems.

The study began by investigating what controls the initial isotopic composition of cold pool water vapor, and it was determined that rain evaporation and equilibration fractionation deplete the downdrafts that generate cold pools in their initial stages, and enrich them in the boundary layer. Mixing tends to have a mostly enriching effect on the downdrafts. The analysis then focused on the propagation of the cold pools and results showed that surface latent heat fluxes enrich the vapor, especially in the first 30 min of the cold pool life cycle, while mixing has a slightly depleting effect. Finally, results showed that, while water vapor isotopes in moist patches could potentially be used to assess the sources of water vapor, the differences between air parcels with different sources might be too small to observe.

This work represents one of the first attempts at using a cloud resolving model and Lagrangian diagnostics to study water vapor isotopes, and the results highlight the benefits that this approach offers. In particular, the ability to explicitly resolve convection and the use of Lagrangian particles allowed a quantification of the roles played by various processes on water vapor isotopes in cold pools. An extension of this analysis to other features of convective systems, such as updrafts and downdrafts, along with a thorough investigation of the sensitivities to external variables, are subject of ongoing work and will create a framework that will further our process-based understanding of atmospheric water vapor isotopes.

Acknowledgments
I am particularly grateful to Peter Blossey for providing the code for this version of SAMiso and helping set it up and run, and for enlightening discussions. I also wish to thank Lisa Welp, Adriana Raudzens Bailey, Martin Singh, Alison Nugent, Camille Risi, and Zhiming Kuang for useful discussions. Finally, I would like to thank two anonymous reviewers whose insightful comments helped improve this manuscript. This research was supported by the National Science Foundation grants AGS-1649819 and AGS-1945972.

Data Availability Statement

The data used for this work is available at https://doi.org/10.5281/zenodo.3837034.

References

Aemisegger, F., Spiegel, J. K., Pfahl, S., Sodemann, H., Eugster, W., & Wernli, H. (2015). Isotope meteorology of cold front passages: A case study combining observations and modeling. *Geophysical Research Letters*, *42*(13), 5652–5660. https://doi.org/10.1002/2015GL063988

Aggarwal, P. K., Romatschke, U., Araguas-Araguas, L., Belachew, D., Longstaffe, F. J., Berg, P., et al. (2016). Proportions of convective and stratiform precipitation revealed in water isotope ratios. *Nature Geoscience*, *9*(8), 624–629. https://doi.org/10.1038/ngeo2739

Araguás-Araguás, L., Froehlich, K., & Rozanski, K. (2000). Deuterium and oxygen-18 isotope composition of precipitation and atmospheric moisture. *Hydrological Processes*, *14*(8), 1341–1355.Retrieved from https://onlinelibrary.wiley.com/doi/abs/10.1002/1099-1085%2820000615%2914%3A8%3C1341%3A%3AAID-HYP983%3E3.0.CO%3B2-Z

Arakawa, A. (2004). The Cumulus Parameterization Problem: Past, Present, and Future. *Journal of Climate*, *17*(13), 2493–2525. https://doi.org/10.1175/1520-0442(2004)017<2493:RATCPP>2.0.CO;2

Bailey, A. (2020). A new lens for evaluating dynamic controls on shallow convection. *Journal of Advances in Modeling Earth Systems*, *12*(8), e2020MS002249. https://doi.org/10.1029/2020MS002249

Bailey, A., Blossey, P. N., Noone, D., Nusbaumer, J., & Wood, R. (2017). Detecting shifts in tropical moisture imbalances with satellite-derived isotope ratios in water vapor. *Journal of Geophysical Research - D: Atmospheres*, *122*(11), 5763–5779. https://doi.org/10.1002/2016JD026222

Bailey, A., Nusbaumer, J., & Noone, D. (2015). Precipitation efficiency derived from isotope ratios in water vapor distinguishes dynamical and microphysical influences on subtropical atmospheric constituents. *Journal of Geophysical Research - D: Atmospheres*, *120*(18), 9119–9137. https://doi.org/10.1002/2015JD023403

Bailey, A., Toohey, D., & Noone, D. (2013). Characterizing moisture exchange between the hawaiian convective boundary layer and free troposphere using stable isotopes in water. *Journal of Geophysical Research - D: Atmospheres*, *118*(15), 8208–8221.Retrieved from https://agupubs.onlinelibrary.wiley.com/doi/abs/10.1002/jgrd.50639

Bechtold, P., Chaboureau, J.-P., Beljaars, A., Betts, A. K., Köhler, M., Miller, M., & Redelsperger, J.-L. (2004). The simulation of the diurnal cycle of convective precipitation over land in a global model. *Quarterly Journal of the Royal Meteorological Society*, *130*(604), 3119–3137. Retrieved from https://rmets.onlinelibrary.wiley.com/doi/abs/10.1256/qj.03.103

Benetti, M., Lacour, J. L., Sveinbjörnsdóttir, A. E., Aloisi, G., Reverdin, G., Risi, C., et al. (2018). A framework to study mixing processes in the marine boundary layer using water vapor isotope measurements. *Geophysical Research Letters*, *45*(5), 2524–2532.Retrieved from https://agupubs.onlinelibrary.wiley.com/doi/abs/10.1002/2018GL077167

Betts, A. K., & Jakob, C. (2002). Evaluation of the diurnal cycle of precipitation, surface thermodynamics, and surface fluxes in the ecmwf model using lba data. *Journal of Geophysical Research*, *107*(D20). LBA 12-1-LBA 12-8. Retrieved from https://agupubs.onlinelibrary.wiley.com/doi/abs/10.1029/2001JD000427

Blossey, P. N., Kuang, Z., & Romps, D. M. (2010). Isotopic composition of water in the tropical tropopause layer in cloud-resolving simulations of an idealized tropical circulation. *Journal of Geophysical Research*, *115*(D24). Retrieved from https://agupubs.onlinelibrary.wiley.com/doi/abs/10.1029/2010JD014554

Böing, S. J., Jonker, H. J. J., Siebesma, A. P., & Grabowski, W. W. (2012). Influence of the Subcloud Layer on the Development of a Deep Convective Ensemble. *Journal of the Atmospheric Sciences*, *69*(9), 2682–2698. https://doi.org/10.1175/JAS-D-11-0317.1

Bony, S., Risi, C., & Vimeux, F. (2008). Influence of convective processes on the isotopic composition (δ18O and δD) of precipitation and water vapor in the tropics: 1. Radiative-convective equilibrium and Tropical Ocean-Global Atmosphere-Coupled Ocean-Atmosphere Response Experiment (TOGA-COARE) simulations. *Journal of Geophysical Research*, *113*(D19). Retrieved from https://agupubs.onlinelibrary.wiley.com/doi/abs/10.1029/2008JD009942

Bony, S., Stevens, B., Frierson, D. M. W., Jakob, C., Kageyama, M., Pincus, R., et al. (2015). Clouds, circulation and climate sensitivity. *Nature Geoscience*, *8*(4), 261–268. https://doi.org/10.1038/ngeo2398

Chandra, A. S., Zuidema, P., Krueger, S., Kochanski, A., de Szoeke, S. P., & Zhang, J. (2018). Moisture distributions in tropical cold pools from equatorial indian ocean observations and cloud-resolving simulations. *Journal of Geophysical Research - D: Atmospheres*, *123*(20), 445–511. Retrieved from https://agupubs.onlinelibrary.wiley.com/doi/abs/10.1029/2018JD028634

Chang, H. K., Gonçalves, R. D., Aggarwal, P. K., Stradioto, M. R., Hespanhol, E. C. B., Sturchio, N. C., et al. (2020). Groundwater isotope ratios reflect convective and stratiform (paleo)precipitation fractions in brazil. *Journal of Hydrology*, *585*, 124801. https://doi.org/10.1016/j.jhydrol.2020.124801

Chen, S.-H., & Sun, W.-Y. (2002). A one-dimensional time dependent cloud model. *Journal of the Meteorological Society of Japan*, *80*(1), 99–118. https://doi.org/10.2151/jmsj.80.99

Collins, W. D., Rasch, P. J., Boville, B. A., Hack, J. J., McCaa, J. R., Williamson, D. L., et al. (2006). The formulation and atmospheric simulation of the community atmosphere model version 3 (cam3). *Journal of Climate*, *19*(11), 2144–2161. https://doi.org/10.1175/JCLI3760.1

Conroy, J. L., Noone, D., Cobb, K. M., Moerman, J. W., & Konecky, B. L. (2016). Paired stable isotopologues in precipitation and vapor: A case study of the amount effect within western tropical pacific storms. *Journal of Geophysical Research - D: Atmospheres*, *121*(7), 3290–3303.Retrieved from https://agupubs.onlinelibrary.wiley.com/doi/abs/10.1002/2015JD023844

Dansgaard, W. (1964). Stable isotopes in precipitation. *Tellus*, *16*(4), 436–468.Retrieved from https://onlinelibrary.wiley.com/doi/abs/10.1111/j.2153-3490.1964.tb00181.x

de Szoeke, S. P., Skyllingstad, E. D., Zuidema, P., & Chandra, A. S. (2017). Cold pools and their influence on the tropical marine boundary layer. *Journal of the Atmospheric Sciences*, *74*(4), 1149–1168. https://doi.org/10.1175/JAS-D-16-0264.1

Dee, S. G., Nusbaumer, J., Bailey, A., Russell, J. M., Lee, J.-E., Konecky, B., et al. (2018). Tracking the strength of the walker circulation with stable isotopes in water vapor. *Journal of Geophysical Research - D: Atmospheres*, *123*(14), 7254–7270.Retrieved from https://agupubs.onlinelibrary.wiley.com/doi/abs/10.1029/2017JD027915

Drager, A. J., Grant, L. D., & Heever, S. C. (2020). Cold pool responses to changes in soil moisture. *Journal of Advances in Modeling Earth Systems*, *12*, n/a(n/a), e2019MS001922. Retrieved from https://agupubs.onlinelibrary.wiley.com/doi/abs/10.1029/2019MS001922

Drager, A. J., & van den Heever, S. C. (2017). Characterizing convective cold pools. *Journal of Advances in Modeling Earth Systems*, *9*(2), 1091–1115.Retrieved from https://agupubs.onlinelibrary.wiley.com/doi/abs/10.1002/2016MS000788

Dütsch, M., Pfahl, S., Meyer, M., & Wernli, H. (2018). Lagrangian process attribution of isotopic variations in near-surface water vapor in a 30-year regional climate simulation over europe. *Atmospheric Chemistry and Physics*, *18*(3), 1653–1669.Retrieved from https://www.atmos-chem-phys.net/18/1653/2018/

Feng, X., Posmentier, E. S., Sonder, L. J., & Fan, N. (2019). Rethinking Craig and Gordon's approach to modeling isotopic compositions of marine boundary layer vapor. *Atmospheric Chemistry and Physics*, *19*(6), 4005–4024.Retrieved from https://acp.copernicus.org/articles/19/4005/2019/

Feng, Z., Hagos, S., Rowe, A. K., Burleyson, C. D., Martini, M. N., & Szoeke, S. P. (2015). Mechanisms of convective cloud organization by cold pools over tropical warm ocean during the amie/dynamo field campaign. *Journal of Advances in Modeling Earth Systems*, *7*(2), 357–381.Retrieved from https://agupubs.onlinelibrary.wiley.com/doi/abs/10.1002/2014MS000384

Fournier, M. B., & Haerter, J. O. (2019). Tracking the gust fronts of convective cold pools. *Journal of Geophysical Research - D: Atmospheres*, *124*(21), 11103–11117.Retrieved from https://agupubs.onlinelibrary.wiley.com/doi/abs/10.1029/2019JD030980

Galewsky, J. (2015). Constraining supersaturation and transport processes in a south american cold-air outbreak using stable isotopologues of water vapor. *Journal of the Atmospheric Sciences*, *72*(5), 2055–2069. https://doi.org/10.1175/JAS-D-14-0352.1

Galewsky, J. (2018). Using stable isotopes in water vapor to diagnose relationships between lower-tropospheric stability, mixing, and low-cloud cover near the island of hawaii. *Geophysical Research Letters*, *45*(1), 297–305.Retrieved from https://agupubs.onlinelibrary.wiley.com/doi/abs/10.1002/2017GL075770

Galewsky, J., & Rabanus, D. (2016). A stochastic model for diagnosing subtropical humidity dynamics with stable isotopologues of water vapor. *Journal of the Atmospheric Sciences*, *73*(4), 1741–1753. https://doi.org/10.1175/JAS-D-15-0160.1

Galewsky, J., Steen-Larsen, H. C., Field, R. D., Worden, J., Risi, C., & Schneider, M. (2016). Stable isotopes in atmospheric water vapor and applications to the hydrologic cycle. *Reviews of Geophysics*, *54*(4), 809–865.Retrieved from https://agupubs.onlinelibrary.wiley.com/doi/abs/10.1002/2015RG000512

Galewsky, J., Strong, M., & Sharp, Z. D. (2007). Measurements of water vapor d/h ratios from mauna kea, hawaii, and implications for subtropical humidity dynamics. *Geophysical Research Letters*, *34*(22). https://doi.org/10.1029/2007GL031330

González, Y., Schneider, M., Dyroff, C., Rodríguez, S., Christner, E., García, O. E., et al. (2016). Detecting moisture transport pathways to the subtropical North Atlantic free troposphere using paired H_2O-δD in situ measurements. *Atmospheric Chemistry and Physics*, *16*(7), 4251–4269.Retrieved from https://acp.copernicus.org/articles/16/4251/2016/

Graf, P., Wernli, H., Pfahl, S., & Sodemann, H. (2019). A new interpretative framework for below-cloud effects on stable water isotopes in vapor and rain. *Atmospheric Chemistry and Physics*, *19*(2), 747–765.Retrieved from https://acp.copernicus.org/articles/19/747/2019/

Guilpart, E., Vimeux, F., Evan, S., Brioude, J., Metzger, J.-M., Barthe, C., et al. (2017). The isotopic composition of near-surface water vapor at the Maïdo observatory (Reunion Island, southwestern Indian Ocean) documents the controls of the humidity of the subtropical troposphere. *Journal of Geophysical Research - D: Atmospheres*, *122*(18), 9628–9650.Retrieved from https://agupubs.onlinelibrary.wiley.com/doi/abs/10.1002/2017JD026791

Hanisco, T. F., Moyer, E. J., Weinstock, E. M., St Clair, J. M. J. M., Sayres, D. S., Smith, J. B., et al. (2007). Observations of deep convective influence on stratospheric water vapor and its isotopic composition. *Geophysical Research Letters*, *34*(4). Retrieved from https://agupubs.onlinelibrary.wiley.com/doi/abs/10.1029/2006GL027899

Henneberg, O., Meyer, B., & Haerter, J. O. (2020). Particle-Based Tracking of Cold Pool Gust Fronts. *Journal of Advances in Modeling Earth Systems*, *12*(5). https://doi.org/10.1029/2019MS001910e2019MS001910

Hurley, J. V., Galewsky, J., Worden, J., & Noone, D. (2012). A test of the advection-condensation model for subtropical water vapor using stable isotopologue observations from mauna loa observatory, hawaii. *Journal of Geophysical Research: Atmospheres*, *117*(D19). https://doi.org/10.1029/2012JD018029

Igel, A. L., Igel, M. R., & van den Heever, S. C. (2015). Make It a Double? Sobering Results from Simulations Using Single-Moment Microphysics Schemes. *Journal of the Atmospheric Sciences*, *72*(2), 910–925. https://doi.org/10.1175/JAS-D-14-0107.1

Khairoutdinov, M. F., & Randall, D. A. (2003). Cloud resolving modeling of the arm summer 1997 iop: Model formulation, results, uncertainties, and sensitivities. *Journal of the Atmospheric Sciences*, *60*(4), 607–625. https://doi.org/10.1175/1520-0469(2003)060<0607:CRMOTA>2.0.CO;2

Khairoutdinov, M., & Randall, D. (2006). High-Resolution Simulation of Shallow-to-Deep Convection Transition over Land. *Journal of the Atmospheric Sciences*, *63*(12), 3421–3436. https://doi.org/10.1175/JAS3810.1

Kuang, Z., & Bretherton, C. S. (2006). A Mass-Flux Scheme View of a High-Resolution Simulation of a Transition from Shallow to Deep Cumulus Convection. *Journal of the Atmospheric Sciences*, *63*(7), 1895–1909. https://doi.org/10.1175/JAS3723.1

Kuang, Z., Toon, G. C., Wennberg, P. O., & Yung, Y. L. (2003). Measured hdo/h2o ratios across the tropical tropopause. *Geophysical Research Letters*, *30*(7). https://doi.org/10.1029/2003GL017023

Kurita, N. (2013). Water isotopic variability in response to mesoscale convective system over the tropical ocean. *Journal of Geophysical Research - D: Atmospheres*, *118*(18), 376–410.Retrieved from https://agupubs.onlinelibrary.wiley.com/doi/abs/10.1002/jgrd.50754

Kurita, N., Noone, D., Risi, C., Schmidt, G. A., Yamada, H., & Yoneyama, K. (2011). Intraseasonal isotopic variation associated with the madden-julian oscillation. *Journal of Geophysical Research: Atmospheres*, *116*(D24). https://doi.org/10.1029/2010JD015209

Langhans, W., & Romps, D. M. (2015). The origin of water vapor rings in tropical oceanic cold pools. *Geophysical Research Letters*, *42*(18), 7825–7834. http://doi.org/10.1002/2015GL065623

Lee, J.-E., & Fung, I. (2008). "Amount effect" of water isotopes and quantitative analysis of post-condensation processes. *Hydrological Processes*, *22*(1), 1–8.Retrieved from https://onlinelibrary.wiley.com/doi/abs/10.1002/hyp.6637

Li, Z., Zuidema, P., & Zhu, P. (2014). Simulated convective invigoration processes at trade wind cumulus cold pool boundaries. *Journal of the Atmospheric Sciences*, *71*(8), 2823–2841. https://doi.org/10.1175/JAS-D-13-0184.1

Lin, Y.-L., Farley, R. D., & Orville, H. D. (1983). Bulk parameterization of the snow field in a cloud model. *Journal of Applied Meteorology and Climatology*, *22*(6), 1065–1092. http://doi.org/10.1175/1520-0450(1983)022<1065:BPOTSF>2.0.CO;2

Lutsko, N. J., & Cronin, T. W. (2018). Increase in Precipitation Efficiency With Surface Warming in Radiative-Convective Equilibrium. *Journal of Advances in Modeling Earth Systems*, *10*(11), 2992–3010.Retrieved from https://agupubs.onlinelibrary.wiley.com/doi/abs/10.1029/2018MS001482

Moore, M., Kuang, Z., & Blossey, P. N. (2014). A moisture budget perspective of the amount effect. *Geophysical Research Letters*, *41*(4), 1329–1335.Retrieved from https://agupubs.onlinelibrary.wiley.com/doi/abs/10.1002/2013GL058302

Nie, J., & Kuang, Z. (2012). Beyond bulk entrainment and detrainment rates: A new framework for diagnosing mixing in cumulus convection. *Geophysical Research Letters*, *39*(21). Retrieved from https://agupubs.onlinelibrary.wiley.com/doi/abs/10.1029/2012GL053992

Noone, D. (2012). Pairing measurements of the water vapor isotope ratio with humidity to deduce atmospheric moistening and dehydration in the tropical midtroposphere. *Journal of Climate*, *25*(13), 4476–4494. https://doi.org/10.1175/JCLI-D-11-00582.1

Noone, D., Galewsky, J., Sharp, Z. D., Worden, J., Barnes, J., Baer, D., et al. (2011). Properties of air mass mixing and humidity in the subtropics from measurements of the d/h isotope ratio of water vapor at the mauna loa observatory. *Journal of Geophysical Research*, *116*(D22), a. Retrieved from https://agupubs.onlinelibrary.wiley.com/doi/abs/10.1029/2011JD015773

Nusbaumer, J., Wong, T. E., Bardeen, C., & Noone, D. (2017). Evaluating hydrological processes in the C ommunity A tmosphere M odel V ersion 5 (C AM5) using stable isotope ratios of water. *Journal of Advances in Modeling Earth Systems*, *9*(2), 949–977. https://doi.org/10.1002/2016MS000839

P. Siebesma, S. Bony, C. Jakob, & B. Stevens (Eds.), Eds., (2020). *Clouds and climate: Climate science's greatest challenge*. Cambridge University Press. https://doi.org/10.1017/9781107447738

Pincus, R., Winker, D., Bony, S., & Stevens, B. (Eds.). (2018). Shallow clouds, water vapor, circulation, and climate sensitivity (Vol. 65 (No. 1). Springer International Publishing.

Pruppacher, H., & Klett, J. (2010). *Microphysics of clouds and precipitation*. Springer Netherlands.

Rio, C., Hourdin, F., Grandpeix, J.-Y., & Lafore, J.-P. (2009). Shifting the diurnal cycle of parameterized deep convection over land. *Geophysical Research Letters*, *36*(7). https://doi.org/10.1029/2008GL036779

Risi, C., Bony, S., & Vimeux, F. (2008). Influence of convective processes on the isotopic composition (δ18O and δD) of precipitation and water vapor in the tropics: 2. Physical interpretation of the amount effect. *Journal of Geophysical Research*, *113*(D19). Retrieved from https://agupubs.onlinelibrary.wiley.com/doi/abs/10.1029/2008JD009943

Risi, C., Bony, S., Vimeux, F., & Jouzel, J. (2010). Water-stable isotopes in the lmdz4 general circulation model: Model evaluation for present-day and past climates and applications to climatic interpretations of tropical isotopic records. *Journal of Geophysical Research*, *115*(D12). Retrieved from https://agupubs.onlinelibrary.wiley.com/doi/abs/10.1029/2009JD013255

Risi, C., Galewsky, J., Reverdin, G., & Brient, F. (2019). Controls on the water vapor isotopic composition near the surface of tropical oceans and role of boundary layer mixing processes. *Atmospheric Chemistry and Physics*, *19*(19), 12235–12260.Retrieved from https://www.atmos-chem-phys.net/19/12235/2019/

Risi, C., Muller, C., & Blossey, P. (2020). What Controls the Water Vapor Isotopic Composition Near the Surface of Tropical Oceans? Results From an Analytical Model Constrained by Large-Eddy Simulations. *Journal of Advances in Modeling Earth Systems*, *12*, e2020MS002106. https://doi.org/10.1029/2020MS002106

Ross, A., Dalziel, S., & Linden, P. (2006). Axisymmetric gravity currents on a cone. *Journal of Fluid Mechanics*, *565*, 227–253. https://doi.org/10.1017/S0022112006001601

Ross, A. N., Tompkins, A. M., & Parker, D. J. (2004). Simple models of the role of surface fluxes in convective cold pool evolution. *Journal of the Atmospheric Sciences*, *61*(13), 1582–1595. https://doi.org/10.1175/1520-0469(2004)061<1582:SMOTRO>2.0.CO;2

Schlemmer, L., & Hohenegger, C. (2014). The Formation of Wider and Deeper Clouds as a Result of Cold-Pool Dynamics. *Journal of the Atmospheric Sciences*, *71*(8), 2842–2858. https://doi.org/10.1175/JAS-D-13-0170.1

Schlemmer, L., & Hohenegger, C. (2016). Modifications of the atmospheric moisture field as a result of cold-pool dynamics. *Quarterly Journal of the Royal Meteorological Society*, *142*(694), 30–42.Retrieved from https://rmets.onlinelibrary.wiley.com/doi/abs/10.1002/qj.2625

Seifert, A., & Heus, T. (2013). Large-eddy simulation of organized precipitating trade wind cumulus clouds. *Atmospheric Chemistry and Physics*, *13*(11), 5631–5645.Retrieved from http://www.atmos-chem-phys.net/13/5631/2013/

Sherwood, S. C., Bony, S., & Dufresne, J.-L. (2014). Spread in model climate sensitivity traced to atmospheric convective mixing. *Nature*, *505*(7481), 37–42. https://doi.org/10.1038/nature12829

Siebesma, A. P., & Cuijpers, J. W. M. (1995). Evaluation of parametric assumptions for shallow cumulus convection. *Journal of the Atmospheric Sciences*, *52*(6), 650–666. https://doi.org/10.1175/1520-0469(1995)052<0650:EOPAFS>2.0.CO;2

Tompkins, A. M. (2001). Organization of tropical convection in low vertical wind shears: The role of water vapor. *Journal of the Atmospheric Sciences*, *58*(6), 529–545. http://dx.doi.org/10.1175/1520-0469(2001)058<0529:OOTCIL>2.0.CO;2

Tompkins, A. M., & Craig, G. C. (1998). Radiative-convective equilibrium in a three-dimensional cloud-ensemble model. *Quarterly Journal of the Royal Meteorological Society*, *124*(550), 2073–2097. Retrieved from https://rmets.onlinelibrary.wiley.com/doi/abs/10.1002/qj.49712455013

Torri, G., & Kuang, Z. (2016a). A Lagrangian Study of Precipitation-Driven Downdrafts*. *Journal of the Atmospheric Sciences*, *73*(2), 839–854. https://doi.org/10.1175/JAS-D-15-0222.1

Torri, G., & Kuang, Z. (2016b). Rain evaporation and moist patches in tropical boundary layers. *Geophysical Research Letters*, *43*(18), 9895–9902. https://agupubs.onlinelibrary.wiley.com/doi/abs/10.1002/2016GL070893

Torri, G., & Kuang, Z. (2019). On cold pool collisions in tropical boundary layers. *Geophysical Research Letters*, *46*(1), 399–407.Retrieved from https://agupubs.onlinelibrary.wiley.com/doi/abs/10.1029/2018GL080501

Torri, G., Kuang, Z., & Tian, Y. (2015). Mechanisms for convection triggering by cold pools. *Geophysical Research Letters*, *42*(6), 1943–1950. Retrieved from https://agupubs.onlinelibrary.wiley.com/doi/abs/10.1002/2015GL063227

Torri, G., Ma, D., & Kuang, Z. (2017). Stable water isotopes and large-scale vertical motions in the tropics. *Journal of Geophysical Research - D: Atmospheres*, *122*(7), 3703–3717.Retrieved from https://agupubs.onlinelibrary.wiley.com/doi/abs/10.1002/2016JD026154

Ungarish, M. (2009). *An introduction to gravity currents and intrusions*. Chapman and Hall/CRC.

Webster, C. R., & Heymsfield, A. J. (2003). Water isotope ratios d/h, 18o/16o, 17o/16o in and out of clouds map dehydration pathways. *Science*, *302*(5651), 1742–1745.Retrieved from https://science.sciencemag.org/content/302/5651/1742

Yang, G.-Y., & Slingo, J. (2001). The Diurnal Cycle in the Tropics. *Monthly Weather Review*, *129*(4), 784–801. https://doi.org/10.1175/1520-0493(2001)129<0784:TDCITT>2.0.CO;2

Zhao, M., Golaz, J.-C., Held, I. M., Ramaswamy, V., Lin, S.-J., Ming, Y., et al. (2016). Uncertainty in model climate sensitivity traced to representations of cumulus precipitation microphysics. *Journal of Climate*, *29*(2), 543–560. https://doi.org/10.1175/JCLI-D-15-0191.1

Zuidema, P., Torri, G., Muller, C., & Chandra, A. (2017). A survey of precipitation-induced atmospheric cold pools over oceans and their interactions with the larger-scale environment. *Surveys in Geophysics*, *38*(6), 1283–1305. https://doi.org/10.1007/s10712-017-9447-x